ELSEVIER

Computerized Medical Imaging and Graphics 28 (2004) 99–108

Computerized Medical Imaging and Graphics

www.elsevier.com/locate/compmedimag

Anterior osteophyte discrimination in lumbar vertebrae using size-invariant features

Maruthi Cherukuri[a], R. Joe Stanley[a,*], Rodney Long[b], Sameer Antani[b], George Thoma[b]

[a]*Department of Electrical and Computer Engineering, University of Missouri-Rolla, 127 Emerson Electric Co. Hall, 1870 Miner Circle, Rolla, MO 65409-0040, USA*

[b]*Communications Engineering Branch, National Library of Medicine, Bethesda, MD, USA*

Received 13 May 2003; accepted 29 September 2003

Abstract

Radiologists often examine X-rays of cervical, thoracic and lumbar vertebrae for determining the presence of osteoarthritis and osteoporosis. For individual vertebra assessment, the boundary increasingly digresses from the general rectangular shape as the vertebra becomes less normal in appearance. For an abnormal vertebra, bony growths ('osteophytes') may appear at the vertebral corners, resulting in a change in the vertebra's shape. Image processing techniques are presented for computing size-invariant, convex hull-based features to highlight anterior osteophytes. Feature evaluation of 714 lumbar spine vertebrae using a multi-layer perceptron yielded normal and abnormal average correct discrimination of 90.5 and 86.6%, respectively.

Keywords: Osteoarthritis; Osteophyte; Neural networks; Image processing; Lumbar spine; X-ray

1. Introduction

Osteoarthritis, or degenerative joint disease, is characterized by the deterioration of joints in the body due to age, injury or disease. It affects more than 16 million Americans, including virtually everyone above the age of 75 [1]. Osteoporosis is a disease that is characterized by low bone mass and structural deterioration of bone tissue, which may result in fragile bones and an increased susceptibility to hip, spine and wrist fractures [2]. From this disease there are over 700,000 vertebral fractures in the US annually [2]. The Lister Hill National Center for Biomedical Communications, an R&D division of the National Library of Medicine (NLM) has built a Web-based Medical Information Retrieval System (WebMIRS) to permit Internet access to databases of X-ray images and associated text data from the National Health and Nutrition Examination Surveys (NHANES) [3]. Part of the initiative to develop WebMIRS is to determine the feasibility of computer-assisted techniques for the analysis of lumbar spine X-ray images. The NHANES X-rays were originally collected for the study of osteoarthritis in the US population; although this paper is concerned with detection of some image features related to that disease, the X-rays are a potential resource for the study of osteoporosis and vertebral fracture through the application of convex hull techniques to measure vertebral deviations.

Radiographs of the spine provide a practical approach for detecting and assessing vertebral abnormalities that may be related to osteoarthritis or osteoporosis. Fig. 1 presents a lumbar spine X-ray image example. The boxed region highlights the lumbar spine vertebrae. The presence of bony growths ('osteophytes') on vertebra corners, disc space narrowing, and subluxation are all features commonly evaluated visually from radiographs that are important to the osteoarthritis research community. Other techniques such as quantitative computed tomography (QCT) [4], dual photon absorptiometry (DPA) [5] and dual energy radiography [6] facilitate accurate assessment of bone mineral content and spine density.

Vertebral morphometry is a commonly used technique to evaluate osteoporosis. In particular, measuring morphometric vertebral deformity is often used in clinical trials for assisting in the diagnosis and follow-up of fractures. Measurement techniques include conventional rulers and

* Corresponding author. Tel.: +1-573-341-6896; fax: +1-573-341-4532.
E-mail address: stanleyr@umr.edu (R.J. Stanley).

0895-6111/$ - see front matter © 2003 Elsevier Ltd. All rights reserved.
doi:10.1016/j.compmedimag.2003.09.002

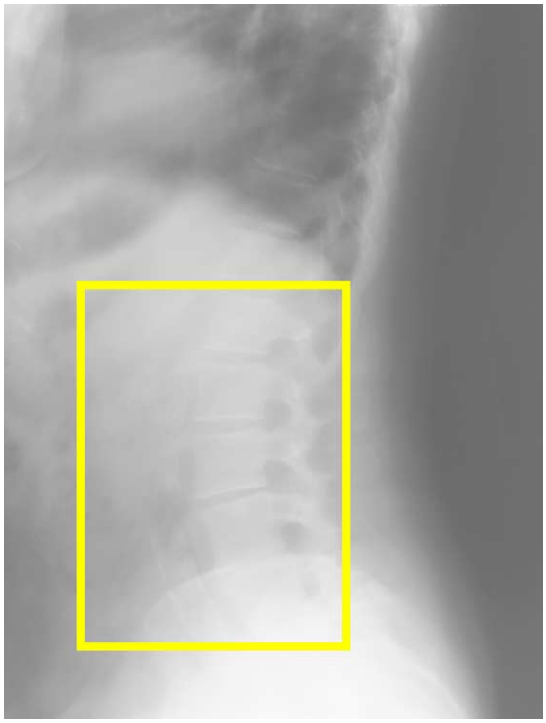

Fig. 1. Lumbar spine X-ray image example from the National Library of Medicine image dataset. Vertebrae are highlighted in the box region.

calipers [7–11] and digitizing tablets [12–15]. Morphometric analysis has encompassed radiographic diagnosis of vertebral fractures based on subjective visual assessment and arbitrarily assessed reductions in vertebral heights [16,17]. Prior studies have utilized vertebral dimensions to establish normal ranges using anterior and posterior vertebral height, percent reduction of anterior compared to posterior height of the same vertebra, the difference in vertebral height of adjoining vertebrae, vertebral width, wedge angle and vertebral angle [7]. Other techniques have been explored assessing the severity of vertebral fractures [7,18,19].

This research focuses on vertebral distortion along the anterior boundary as an indicator of osteophytes. Fig. 2 presents three examples of anterior osteophytes in lumbar vertebrae with osteophytes in the upper left-hand corner (a), osteophytes in the lower left-hand corner (b), and osteophytes in both left-hand corners (c). Fig. 3 shows a normal vertebra (left-hand side is the anterior side) for comparison purposes. The presence of osteophytes is significant because it may be related to degeneration in the attachment of the outer annular fibers of the disc to the vertebral endplate. This degeneration may allow the vertebra to slip to the anterior or to both the anterior and the side [20]. Vertebra distortion based on anterior osteophytes results in a deviation from the characteristic rectangular vertebral shape, which tends to be convex.

In prior research, image processing techniques were investigated to compute features along the anterior boundary of cervical spine vertebrae for differentiating normal vertebrae from vertebrae with abnormal osteophytes [21]. The features examined were radius-of-curvature-and grayscale gradient-based features computed along the anterior boundary of cervical spine vertebrae. The radius of curvature-based features highlight the relative constriction along the anterior boundary between normal and abnormal vertebrae. The grayscale border gradient features examine the grayscale contrast difference between the vertebral interior and exterior along the boundary. The primary difficulty with the radius-of-curvature features was that they were not adaptive to vertebral size. In this research, size-invariant convex hull features are introduced to detect anterior osteophytes in lumbar spine vertebra. Size-invariant features are investigated in order to facilitate the direct comparison of vertebrae between radiographs.

The convex hull of a data set of points is the smallest convex set of points that includes the data set of points [22]. The convex hull is determined from a vertebra's boundary points in order to compute features characterizing the vertebra's shape. Examining Figs. 2 and 3, a normal vertebra generally has rectangular shape and tends to be convex. Thus, the convex hull for a lumbar spine without anterior osteophytes is anticipated to be similar to its original shape on the anterior side. Inspecting Fig. 2, the protrusion region along the anterior side of the vertebra contains osteophytes, making the vertebra shape concave. Four size-invariant features are determined based on comparing a filled vertebra with its filled convex hull.

A standard multi-layer perceptron (MLP) is used to evaluate the features for osteophytes discrimination on a substantial lumbar vertebrae data set. The outline for the remainder of the paper is to present: (1) the algorithm for osteophyte detection in lumbar vertebrae, (2) experiments

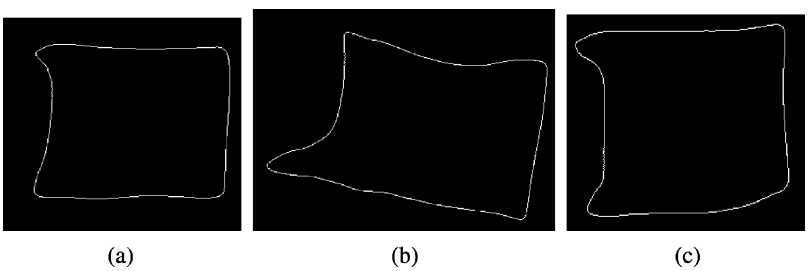

Fig. 2. Three examples of anterior osteophytes in lumbar vertebrae with osteophytes in upper left-hand corner (a), osteophytes in the lower left-hand corner (b), and osteophytes in both left-hand corners (c).

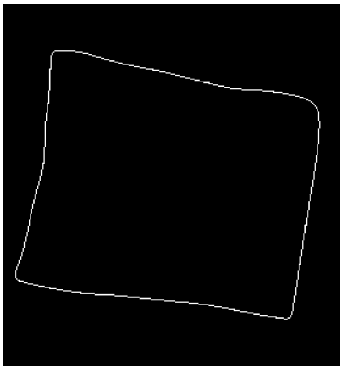

Fig. 3. Example for normal lumbar vertebra without anterior osteophytes. The left-hand side is the anterior side of the vertebra shown.

performed, (3) experimental results and discussion, and (4) conclusions.

2. Algorithm for osteophytes discrimination in lumbar vertebrae

In this research, image analysis techniques are investigated for detecting and differentiating normal and abnormal (i.e. having osteophytes) lumbar spine vertebrae. For individual vertebra analysis manual vertebral segmentation is performed. The steps for manual vertebra segmentation, vertebral feature calculations, and vertebral discrimination are presented in following sections. Fig. 4 shows the algorithm overviewing the operations performed on each vertebra for feature calculations.

2.1. Vertebral boundary determination

For the lumbar spine X-ray images used in this research, an expert radiologist identified and marked 7–9 points along the vertebra's boundary. Specifically, the radiologist marked the top and bottom points of the anterior and posterior sides, the midpoints of the top and bottom sides, the anterior midpoint, and up to two points near the anterior corners, where osteophytes (if any) were located. For vertebra segmentation, vertebral boundary points were manually chosen and a second order B-spline algorithm [23] was used to connect the points to generate a closed boundary. In order to facilitate manual boundary point selection, the expert radiologist selected points were superimposed onto the histogram stretched [24] original X-ray image. Histogram stretching of the original image improved the contrast between the vertebral boundaries and the surrounding background. Based on experimentation, approximately 55 manually chosen points provided a reasonable vertebral boundary representation for feature analysis. Fig. 5 presents an example of histogram stretched X-ray image with the radiologist points superimposed (a) and a reference vertebra containing the selected positions along the vertebra boundary that the radiologist would label (b). The arrows in Fig. 5(a) point to two radiologist-provided points. Figs. 2 and 3 present image examples of vertebral boundaries determined using the manual and B-Spline-based procedure.

2.2. Vertebral features calculation

In this section, four convex hull-based features are investigated for vertebra discrimination. The following notation is used for defining the features. Let I denote the $M \times N$ intensity lumbar spine X-ray image, where $1 \leq x \leq M$ and $1 \leq y \leq N$. Let V denote a lumbar vertebra within an X-ray image with area A_v such that

$$\mathrm{V} = \begin{cases} 1 & \text{if } (x, y) \text{ is on or inside the vertebra boundary} \\ 0 & \text{otherwise} \end{cases}$$

For the lumbar spine X-ray image data examined, the lumbar vertebrae examined in each X-ray image include L3-L5. The convex hull for V is determined using the quick convex hull algorithm [22]. Let C denote the resulting filled convex hull for vertebra V such that

$$\mathrm{C} = \begin{cases} 1 & \text{if } (x, y) \text{ is on or inside the convex hull boundary for V} \\ 0 & \text{otherwise} \end{cases}$$

Let E denote the set of exclusive-OR points between V and C such that $E(x, y) = \mathrm{V}(x, y) \oplus \mathrm{C}(x, y)$. E is expected to contain one or more connected regions, for each concave vertebral side. Using 8-connectivity, let k denote the number of unique connected components within E.

The four features used for detecting anterior osteophytes include: (1) the ratio of the vertebral area to the convex hull area, (2) the ratio of the exclusive-OR area to the convex hull area, (3) the ratio of the exclusive-OR area on the vertebra's anterior side to the vertebra area and (4) the ratio of the area of the largest connected region from the exclusive-OR regions on the anterior side of the vertebra to the vertebra area. For the data set examined in this research, osteophytes, if present, are found on the anterior side of the vertebra, with the left-hand side of each

Determine edge image
For each vertebra
    Manually label border points using edge image and radiologist-labeled points as a guide
    Draw vertebral border from manually labeled border points
    Compute size-invariant convex hull features set
EndFor

Fig. 4. The algorithm over view of the operations performed on each vertebra for feature calculations.

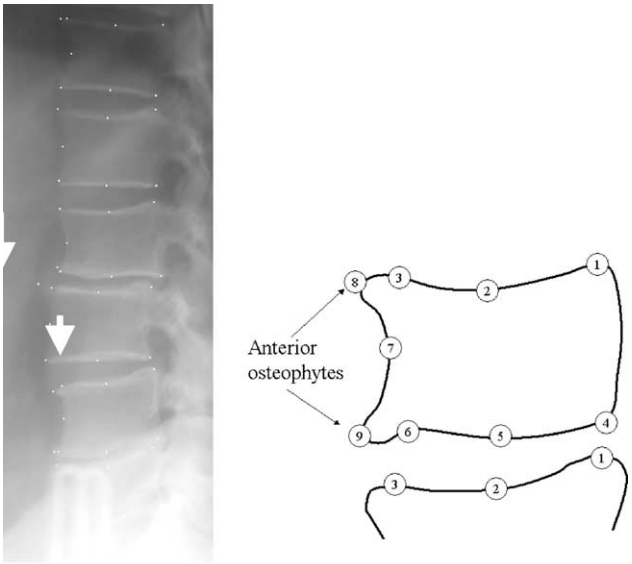

Fig. 5. Image examples showing expert radiologist selected points used in the manual point selection process around the vertebra boundary. (a) Histogram stretched original image and expert radiologist selected points. (b) Labeled points that the expert radiologist selects to characterize a vertebra. Points 8 and 9 are locations for abnormal osteophytes.

vertebra corresponding to the anterior side and the right-hand side corresponds to the posterior side. The goal with feature extraction is to highlight protrusion regions on the anterior side of the vertebra that are characteristic of osteophytes. The ratios of the exclusive-OR area to the filled convex hull and the vertebra area, respectively, are intended to quantify the variation of the vertebral shape from the vertebra's ideal rectangular shape. The exclusive-OR regions represent concave regions around the vertebra's periphery. The final exclusive-OR-based feature focuses on the anterior side of the vertebra for finding the largest concave region and comparing the size of the concavity to the vertebra size in order to highlight the location of the largest protrusion region. The features examined provide size-invariant measures of the deviation of the filled convex hull from the original filled vertebra. The purpose for exploring size-invariant features is to enable the direct comparison of different vertebrae within the same X-ray image (i.e. the same patient) and vertebrae from different images (i.e. different patients).

For the initial feature, the ratio of the vertebral area to the filled convex hull is denoted as R and is defined as $R = A_V/A_C$. The ratio of the exclusive-OR area to the filled convex hull area is denoted as T and is defined as $T = A_E/A_C$. In order to illustrate this feature, Fig. 6 presents the exclusive-OR for a normal lumbar vertebra, and Fig. 7 provides the exclusive-OR of an abnormal vertebra with anterior osteophytes on the lower left-hand side. From Figs. 6 and 7, there are a number of

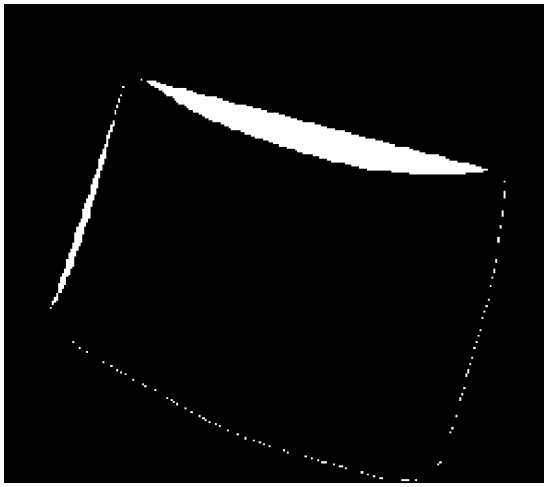

Fig. 6. The exclusive-OR operation between original vertebra and its convex hull image for a normal vertebra.

disconnected regions in the exclusive-OR between the filled vertebra and its corresponding filled convex hull.

The following procedure is used to compute the final two exclusive-OR-based features. The centroid location, (x_c, y_c), is calculated for the vertebra V. Second, the connected regions within E are connected component labeled [24]. Third, the original XY plane is shifted to new X^1Y^1 plane for V, which is centered at the centroid location with the axes parallel to the original XY axes.

The third feature computed is the ratio of the exclusive-OR area on the vertebra's anterior side to the vertebral area. Connected components in E that touch or are entirely located on the right-hand side of the X^1Y^1 plane (i.e. positive X^1 half-plane) are removed. In other words, any connected component in E with one or more pixels on the Y^1 axis or the negative X^1 axis are removed. These connected components are considered as part of the posterior portion of the vertebra and are not related to anterior osteophytes. Let G denote the number of

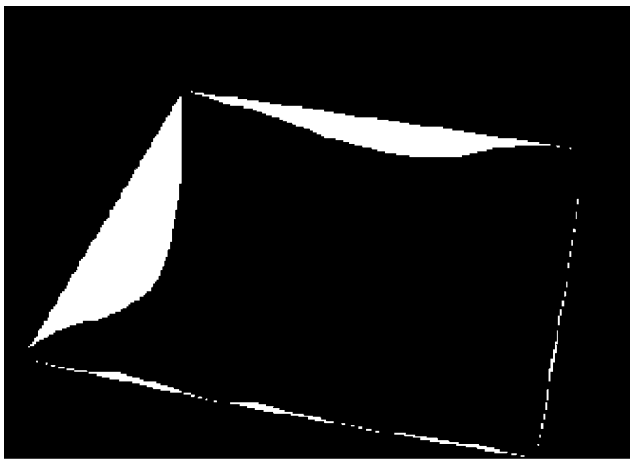

Fig. 7. The exclusive-OR operation between original vertebra and its convex hull image for an abnormal vertebra with anterior osteophytes (lower left-hand side).

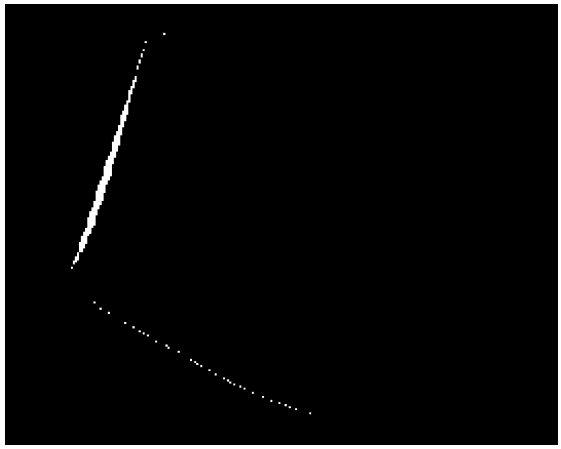

Fig. 8. The exclusive-OR area after removing the posterior side of a normal vertebra. (example for a normal vertebra).

Fig. 9. The exclusive-OR area after removing the posterior side of an abnormal vertebra.

connected components remaining in the negative X^1 plane (i.e. anterior side). Let $H = \{h_1, h_2, \ldots, h_G\}$ refer to the set of connected components remaining with areas given by A_h, for $1 \leq i \leq G$. Then, the ratio of the exclusive-OR area on the vertebra's anterior side to vertebral area is denoted as U and is defined as $U = \sum_{i=1}^{G} A_{h_i}/A_{\mathrm{V}}$. The final convex hull-based feature is based on finding the largest connected component on the anterior side. Then, the ratio of the largest connected region from the exclusive-OR regions on the anterior side of the vertebra to the vertebral area is denoted as F and is defined as $F = \max_i (A_{h_{o_i}})/A_{\mathrm{V}}$, where $1 \leq i \leq G$. Note that $G = 1$ for the lumbar vertebrae examined. Figs. 8 and 9 show examples of the exclusive-OR area after removing the posterior portion of the image for normal and abnormal vertebrae, respectively.

3. Experiments performed

3.1. Data set description

A data set of lumbar spine X-ray images was used for algorithm development. For classification purposes, vertebrae are labeled normal or abnormal (i.e. those that contain anterior osteophytes). From these X-ray images, borders were manually determined for 714 individual vertebrae, including 357 normal and 357 abnormal vertebrae using lumbar vertebrae L3-L5. The four convex hull-based features are computed for each vertebra.

3.2. Schemes for vertebral classification

In order to evaluate which features contribute most significantly to correct vertebrae discrimination, the following experiments are performed. Standard MLPs [25] were used to evaluate all four convex hull-based features and the features individually for vertebrae discrimination. The Matlab 6.1 implementation for the MLP was used, using the built-in functions for training and testing modes. Twenty randomly generated training, cross-validation and test sets were generated for evaluating the vertebral features using about 80% of the data for training, 5% for cross-validation and the remaining 15% for testing. From the data set examined, 572 vertebrae used for training (286 normal and 286 abnormal), 34 for cross-validation (17 normal and 17 abnormal) and 108 vertebrae for testing (54 normal and 54 abnormal) purposes. Feature normalization was performed by computing the mean and standard deviation of each feature from the training set. Each feature was normalized for the training, cross-validation and test sets by subtracting the mean and dividing by the standard deviation using the mean and standard deviation feature values obtained from the training set.

The process for neural network training for each training/cross-validation/test set is to train the neural network for an initial five epochs (iteration through the entire training set five times), retaining the neural network weights. Then, MLP training is performed one epoch at a time, 'testing' the neural network using the cross-validation set to compute the percentage of correctly classified vertebrae for that epoch. For cross-validation testing, T denotes the MLP cross-validation output threshold that yields the maximum percent correct vertebral classification for the current epoch. Based on the approach used for training the MLP, a vertebra with a feature vector that generates MLP output values less than T is labeled abnormal, otherwise the vertebra is called normal. The process is repeated, continuing to update the neural network weights for each epoch, until either: (1) the correct classification rate for the cross-validation set has not improved for five consecutive epochs or (2) the correct classification rate for the cross-validation set is lower than for the previous epoch. The MLP weights obtained from the previous epoch for the two terminating conditions described above are used in testing the neural network. $T_{\max}$ denotes the threshold obtained from the cross-validation set corresponding to the epoch at which MLP training was

terminated. The threshold T_{max} is applied to the test set for determining the correct classification rate for normal and abnormal vertebrae. T_{max} is also applied to the training set to compute the correct training normal and abnormal classification rates.

4. Experimental results and discussion

4.1. Image regions used for feature calculations

Four convex hull-based features were computed for each manually segmented vertebra. Fig. 10 presents an example of the vertebral image regions (abnormal vertebra shown) used for computing the four features. Fig. 10(a) gives the filled vertebra. Fig. 10(b) provides the filled convex hull for the vertebra in Fig. 10(a). Fig. 10(c) presents the exclusive-OR of the filled vertebra and its filled convex hull. Fig. 10(d) gives the connected components from (c) that are on the anterior side of the vertebra. Fig. 10(e) provides the largest connected component from (c). R is computed using areas of (a) and (b). T is found based on the areas from (a) and (c). U is calculated using the areas from (d) and (b). F is obtained based on the areas from (e) and (b).

4.2. Vertebra discrimination results

The initial set of experiments evaluated the discrimination capability of the four convex hull-based features using the MLP approach described in Section 4.1 Twenty randomly generated training, cross-validation and test sets were generated for feature evaluation. The following MLP parameters were experimentally determined: (1) architecture of 4 inputs, 4 nodes in a single hidden layer and one output ($4 \times 4 \times 1$), (2) learning rate of 0.03, (3) momentum of 0.85, (4) sigmoid transfer functions at the input and all hidden layers, and (5) a linear transfer function at the output layer. The threshold T_{max} is determined for each randomly generated training, cross-validation and test set. The number of epochs used for MLP training is based on identifying the epoch for which the cross-validation classification results

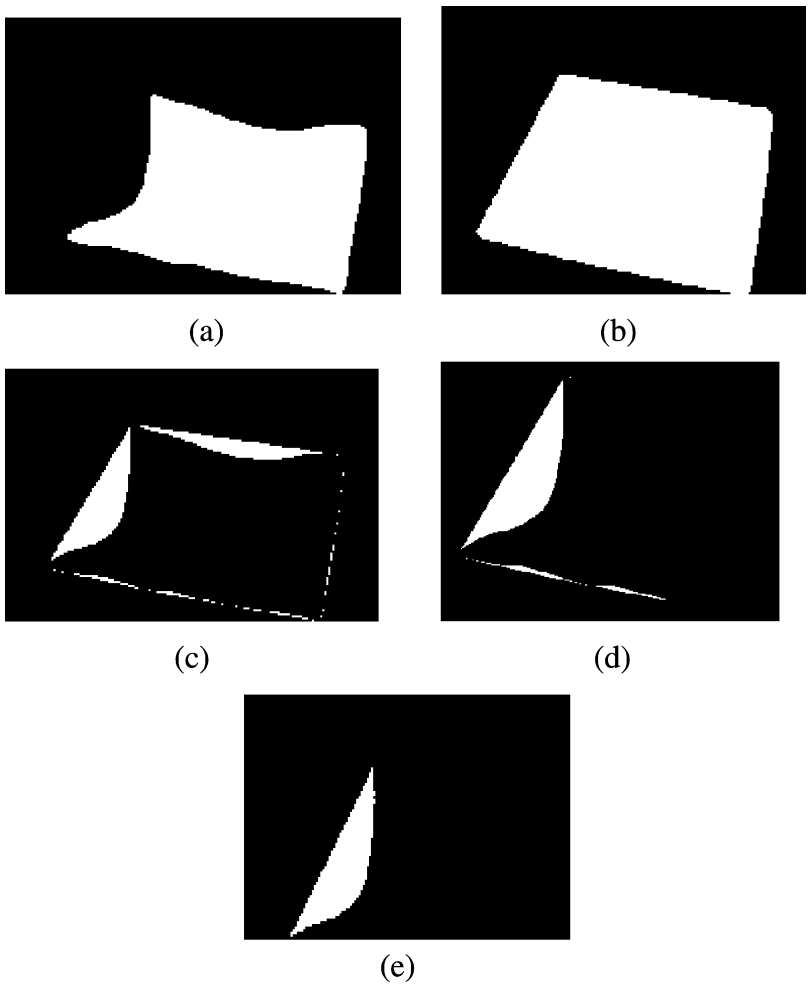

Fig. 10. Example of images used for feature calculations for an abnormal vertebra. (a) Filled vertebra image. (b) Filled convex hull image. (c) Exclusive-OR image of (a) and (b). (d) Exclusive-OR image region on vertebra's anterior side. (e) Connected component with largest area on anterior side.

Table 1
MLP training and test discrimination results for four convex hull-based features for 20 randomly generated training, cross-validation and test sets, including the mean and standard deviation results. The threshold T_{max} is shown for each iteration

Iteration	Threshold T_{max}	Training results		Test results	
		% Correct normal	% Correct total	% Correct normal	% Correct abnormal
1	0.40	87.41	93.01	90.74	88.89
2	0.40	87.41	90.56	79.63	98.15
3	0.40	88.81	91.26	87.04	90.74
4	0.41	88.81	90.91	83.33	90.74
5	0.40	87.06	92.31	88.89	90.74
6	0.40	88.81	89.86	88.89	90.74
7	0.55	92.31	87.41	83.33	94.44
8	0.57	90.91	86.71	96.30	83.33
9	0.40	90.21	90.21	85.19	87.04
10	0.59	92.31	84.27	98.15	87.04
11	0.56	91.61	86.36	90.74	87.04
12	0.45	90.56	89.51	87.04	90.74
13	0.40	90.91	89.16	88.89	92.59
14	0.40	88.11	91.61	92.59	87.04
15	0.40	88.46	91.61	87.04	98.15
16	0.40	89.51	90.21	94.44	90.74
17	0.55	91.61	89.16	85.19	85.19
18	0.40	89.51	88.46	88.89	87.04
19	0.40	86.71	91.96	88.89	96.30
20	0.40	88.46	91.26	87.04	92.59
Mean	89.48	89.79	88.61	90.46	89.48
Standard deviation	1.75	2.23	4.47	4.09	1.75

satisfied one of the two conditions described in Section 3. Experiments performed.

Table 1 below presents the training and test results for the four convex hull-based features for the 20 randomly generated training, cross-validation and test sets with the mean and standard deviation training and test results. The first column shows the randomly generated training, cross-validation, test set iteration number. The second column gives the threshold value T_{max} used for determining the correct normal and abnormal vertebrae classification rates for the corresponding training and test sets. T_{max} is chosen experimentally with cross-validation data set to minimize the classification errors. Columns 3 and 4 provide the training normal and abnormal discrimination rates. Columns 4 and 5 present the test normal and abnormal discrimination rates.

From Table 1, the average and standard deviation training classification rates are 89.48 and 1.75% for normal vertebrae and 89.79 and 2.23% for abnormal vertebrae, respectively. The corresponding average and standard deviation test results are 88.61 and 4.47% for normal vertebrae and 90.46 and 4.09% for abnormal vertebrae, respectively. The low standard deviations for the training and test results indicate consistency in the results obtained. The normal and abnormal vertebrae test results show that the convex hull-based features can be used to successfully discriminate normal vertebrae from vertebrae containing anterior osteophytes. The convex hull-based features quantify concavities in the vertebra shape in comparison to the vertebral area or the vertebra's filled convex hull area. The primary difficulty with vertebra area, filled convex hull area and exclusive-OR area features, R and U, is that these features are global features based on the entire vertebra. In contrast, the maximum exclusive-OR region feature (F) focuses on the anterior side of the vertebra, where the osteophytes may be present. The feature T is examined in order to determine if there is detectible shape variation between normal vertebrae and vertebrae with anterior osteophytes.

Each feature is evaluated individually used an MLP in order to discern discrimination capability of the global vertebral features (R and U) to the local vertebra features (T and F). For the individual features, the same 20 randomly generated training/cross-validation/test sets and the same approach for MLP training were used. The MLP architecture used was simply 1 input and 1 output, with no hidden layer. Table 2 shows the average and standard deviation of twenty random data sets training and test results for each individual feature. The first column contains the feature evaluated (R, U, T, F) and all features for the mean and standard deviation results over the 20 randomly generated training/cross-validation/test sets. Columns 2 and 3 present the training average and standard deviation normal and abnormal vertebral classification results, respectively. Columns 3 and 4 give

Table 2
Average and standard deviation MLP training and test discrimination results for 20 randomly generated training, cross-validation and test sets for individual features. The average and standard deviation training and test results for all four features from Table 1 are shown for comparison

Feature	Training set		Test set	
	% Correct normal	% Correct abnormal	% Correct normal	% Correct abnormal
Mean				
R	59.41	76.42	57.78	76.39
U	61.47	70.58	60.19	71.11
V	65.93	86.10	65.28	85.28
F	88.81	90.44	87.87	92.22
All features	89.48	89.79	88.61	90.46
Standard deviation				
R	27.10	15.32	26.40	16.39
U	26.82	27.04	26.77	27.67
V	34.55	21.09	33.94	21.82
F	1.50	1.45	5.08	4.27
All features	1.75	2.23	4.47	4.09

the test average and standard deviation normal and abnormal vertebral classification results, respectively. The average and standard deviation training and test results for all four features from Table 1 are shown for comparison purposes.

The results presented in Tables 1 and 2 lead to several observations. First, feature F provides the highest average test results for the convex hull-based features. From Table 2, one can observe the mean and standard deviation results for each feature. The standard deviation for the results from F feature show the consistency in the feature's performance. From Table 2, the results for all four features provide a slightly lower standard deviation than for feature F by itself. Fig. 11 shows the principal component analysis (PCA) results for all four features. The figure shows the dominance of one feature over the other three features, which caused the all-feature neural network to give about the same performance when compared to feature F.

Features R and T are based on the complete vertebra (i.e. including the posterior side of the image). From Figs. 6 and 7, one can observe the significant area on the top portion of the vertebra after exclusive-OR between the filled vertebra and its filled convex hull. The numerator for feature F is the area of the largest connected component on the vertebra's anterior side from the exclusive-OR of the filled vertebra and its filled convex hull. This corresponds to the largest concave region along the vertebra's periphery. A vertebra with osteophytes contains one or more protrusion regions, causing the vertebra to deviate from the characteristic rectangular shape. The protrusion regions introduce concavities in the vertebra's shape. The convex hull-based features investigated attempt to quantify the degree of the vertebra's concavity with respect to the vertebra's filled convex hull. One potential reason that feature F outperforms the other features so significantly is that features R, T, and U include regions on the top and bottom of the vertebra in the numerators for the respective feature calculations. The top and bottom regions of the vertebra are often curved, providing concave regions in the vertebra. These concave regions may provide inconsistencies in the features R, T, and U.

Second, the four convex hull-based features can be successfully applied to osteophyte detection for lumbar vertebrae in the data set examined. The convex hull-based features are size-invariant and can be applied to other data

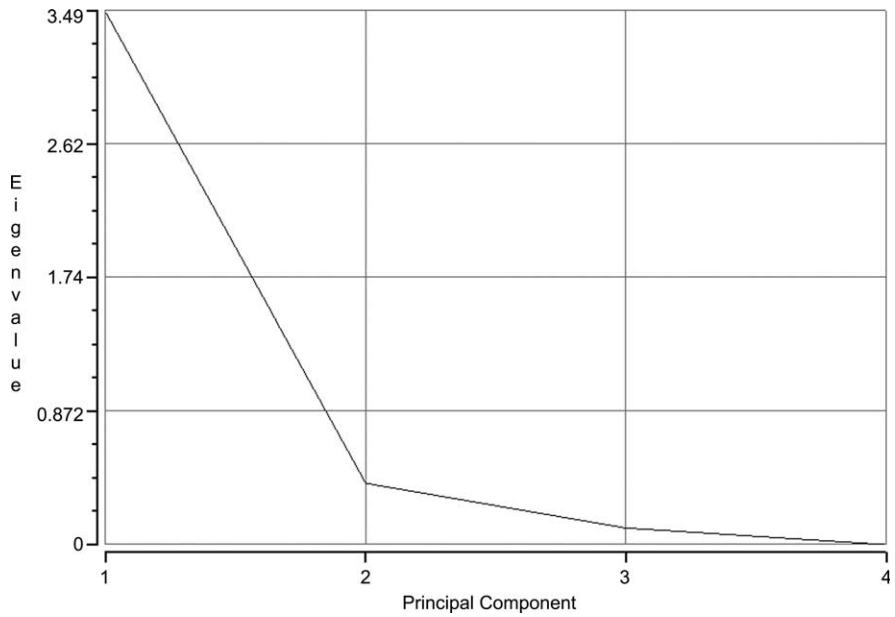

Fig. 11. Principal component analysis results for all four size-invariant, convex hull-based features.

sets for osteophyte analysis. From Tables 1 and 2, the average normal and abnormal vertebrae correct test discrimination results for all four features are 88.61 and 90.46%, respectively. These results are quite similar to the average discrimination results for feature F by itself with average normal and abnormal correct test results 87.87 and 92.22%, respectively. However, the average standard deviation results from Tables 1 and 2 for all four features are slightly lower than for feature F by itself. The convex hull-based features introduced in this research provide a novel approach for lumbar vertebrae osteophyte analysis. The experimental results demonstrate the utility of these features for discriminating normal vertebrae from vertebrae containing anterior osteophytes.

Finally, size-invariant features are needed in order to assess a vertebra's relative deviation from the characteristic rectangular shape for a vertebra. A normal vertebra showing the characteristic rectangular shape is expected to be convex in shape. An abnormal vertebra containing osteophytes contains a protrusion region at one or more of the vertebra tips, resulting in a deviation from the typical rectangular, convex shape.

5. Summary

In this research, image analysis techniques were presented for anterior osteophyte assessment in lumbar vertebrae. Specifically, four size-invariant, convex hull-based features were investigated for differentiating normal vertebrae from vertebrae containing anterior osteophytes. The convex hull-based features quantify the variation in a vertebra's shape from a typical convex shape, emphasizing the variation on the anterior side of the vertebra. Using a MLP, experimental results showed that the ratio of the largest connected component on the anterior side from the exclusive-OR between the filled vertebra and its filled convex hull, denoted as F, provided the highest and most consistent results of the four convex hull-based features. The experimental results demonstrate that the convex hull-based features can be successfully applied to normal and abnormal (i.e. contain anterior osteophytes) vertebrae discrimination. Furthermore, the features investigated are size-invariant and can be applied to vertebra analysis in different X-ray images.

References

[1] Fact Sheet: osteoarthritis. American College of Rhematology, Atlanta, GA; 1994.

[2] Disease statistics: fast Facts. Website for the National Osteoporosis Foundation. www.nof.org/osteoporosis/stats.htm; May 2003.

[3] Long LR, Thoma GR. Image query and indexing for digital X-rays. SPIE Conference on Storage and Retrieval for Image and Video Databases VII, San Jose, CA. Proc SPIE 1999;3656:12–21.

[4] Genant HK, Ettinger B, Harris ST, Block JE, Steiger P. Quantitative computed tomography in assessment of osteoporosis. In: Riggs BL, Melton LJ, editors. Osteoporosis: etiology, diagnosis and management. New York: Lippincott Williams & Wilkins Publishers. 1988:221–49.

[5] Mazess RB, Wahner HM. Nuclear medicine and densitometry. In: Riggs BL, Melton LJ. Osteoporosis: etiology, diagnosis and management. New York: Lippincott Williams & Wilkins Publishers. 1988:251–95.

[6] Sartoris DJ, Resnick D. Dual energy radiographic absorptiometry for bone densitometry: current status and perspective. AJR 1989;152: 242–6.

[7] Hedlund LR, Gallagher JC. Vertebral morphometry in diagnosis of spinal fractures. Bone Miner 1988;5:59–67.

[8] Gallagher JC, Hedlund LR, Stoner S, Meeger C. Vertebral morphometry: normative data. Bone Miner 1988;4:189–96.

[9] Minne HW, Leidig G, Wuster C, Siromachkostov L, Baldauf G, Bickel R, Sauer P, Lojen M, Ziegler R. A new developed spine deformity index (SDI) to quantitate vertebral crush fractures in patients with osteoporosis. Bone Miner 1988;3:335–49.

[10] Raymakers JA, Kapelle JW, van Beresteijn ECH, Duursma SA. Assessment of osteoporotic spine deformity: a new method. Skeletal Radiol 1990;19:91–7.

[11] Eastell R, Cedel SL, Wahner HW, Riggs BL, Melton LJ. Classification of vertebral fractures. J Bone Miner Res 1991;6:207–15.

[12] McCloskey EV, Spector TD, Eyres KS, Fern ED, O'Rourke N, Vasikaran S, Kanis JA. The assessment of vertebral deformity: a method for use in population studies and clinical trials. Osteoporosis Int 1993;3:138–47.

[13] Saur P, Leidig G, Minne HW. Spine deformity index (SDI) versus other objective procedures of vertebral fracture identification in patients with osteoporosis: a comparative study. J Bone Miner Res 1991;6:227–38.

[14] Smith-Bindman R, Cummings SR, Steiger P, Genant HK. A comparison of morphometric definitions of vertebral fracture. J Bone Miner Res 1991;6:25–34.

[15] Ross PD, Davis JW, Epstein RS, Wasnich RD. Ability of vertebral dimensions from a single radiograph to identify fractures. Calcif Tissue Int 1992;51:95–9.

[16] Ott SM, Kilocyne RF, Chesnut III CH. Ability of four different techniques of measuring bone mass to diagnose vertebral fractures in postmenopausal women. J Bone Min Res 1987;2:201–10.

[17] Barnett E, Nordin BEC. The radiological diagnosis of osteoporosis: a new approach. Clin Radiol 1960;11:166–74.

[18] Reinbold WD, Genant HK, Reiser UJ, Harris ST, Ettinger B. Bone mineral content in early-post-menopausal and postmenopausal osteoporotic women: comparison of measurement methods. Radiology 1986;160:469–79.

[19] Meunier PJ, Bressot C, Vignon E. Radiological and histological evolution of post-menopausal osteoporosis treated with sodium fluoride-vit D-calcium; preliminary results. In: Donath A, Baud CA, editors. Fluoride and bone. Bern: Han-Huber; 1978. p. 263–76.

[20] Taylor JA, Resnick D. The aging spine: radiographic-pathologic correlation. In: Genant HK, Jergas M, van Juijk C, editors. Vertebral fracture in osteoporsis, research group. San Francisco, CA: University of California at San Francisco; 1995.

[21] Stanley RJ, Long R. A radius of curvature-based approach to cervical spine vertebra image analysis. Copper Mountain, CO. Proc 38th Annu Rocky Mountain Bioengng Symp 2001;37:385–90.

[22] Barber CB, Dobkin DP, Huhdanpaa HT. The Quickhull algorithm for convex hulls. ACM Trans Math Software 1996;22(4):469–83.

[23] Zhang Z, Stoecker WV, Moss RH. Border detection of digitized skin tumor images. IEEE Trans Med Imaging 2000;19(11):1128–43.

[24] Haralick RM, Shapiro LG, Computer and robot vision, vol. 1. New York, NY: Addison-Wesley; 1992.

[25] Zurada JM. Introduction to artificial neural systems. New York, NY: West Publishing; 1992.

Maruthi Cherukuri received his primary and secondary education in Viyyampeta, India. He received his Bachelor's degree in Electronics and Instrumentation Engineering in June 2000 from Andhra University, India. He received his Master's degree in Computer Engineering from the University of Missouri-Rolla in August 2003.

R. Joe Stanley received the B.S.E.E. and M.S.E.E. degrees in electrical engineering and a PhD degree in Computer Engineering and Computer Science from the University of Missouri-Columbia. As a graduate student at the University of Missouri-Columbia, he worked under training grants from the National Library of Medicine and the National Cancer Institute. Upon completing his doctoral study, he served as Principal Investigator for the Image Recognition program at Systems &Electronics, Inc. in St Louis, MO. He is currently an Assistant Professor in the Department of Electrical and Computer Engineering at the University of Missouri-Rolla. His research interests include signal and image processing, pattern recognition and automation. Dr Stanley is a Senior Member of the IEEE and a member of NAFIPS.

L. Rodney Long is an electronics engineer for the Communications Engineering Branch in the Lister Hill National Center for Biomedical Communications, a research arm of the National Library of Medicine. He has held his current position since 1990. Prior to his current job, he worked for 14 years in industry as a software developer and as a systems engineer. His research interests are in image processing and scientific/biomedical databases, with emphasis on the content-based retrieval of medical images. He has an M.A. in applied mathematics from the University of Maryland.

Sameer Antani is with the Lister Hill National Center for Biomedical Communications at the National Library of Medicine. He earned his B.E. (Computer) degree from the University of Pune, India, in 1994; and M. Eng. and PhD degrees in Computer Science and Engineering from The Pennsylvania State University in 1998 and 2001, respectively. He is interested in Content Analysis of Visual Information, Multimedia Databases, Medical Image Databases, Computer Vision, Document Image Analysis, and Computer Graphics. His current projects include topics on (complete and partial) shape representation and similarity algorithms for spine X-ray image retrieval, color- and texture-based segmentations of acetowhitened images of the uterine cervix, and image indexing algorithms, among others. Sameer is a member of the IEEE and the IEEE Computer Society.

George R. Thoma is Chief of the Communications Engineering Branch of the Lister Hill National Center for Biomedical Communications, a research and development division of the US National Library of Medicine. In this capacity, he directs R&D programs in document image analysis and understanding, biomedical image processing, image compression, automated document image delivery, digital X-ray archiving, animated virtual books, and high speed image transmission. He earned a B.S. from Swarthmore College, and the M.S. and PhD from the University of Pennsylvania, all in electrical engineering. Dr Thoma is a Fellow of the SPIE, the International Society for Optical Engineering.